# ShearMoFit: A Dual-Plane Ultrasound Shear Wave Motion Cleaning Technique

MD Jahin Alam<sup>1</sup>, Md Ashikuzzaman<sup>1</sup>, and Muyinatu A. Lediju Bell<sup>1,2,3</sup>

<sup>1</sup>Department of Electrical and Computer Engineering, Johns Hopkins University, Baltimore, MD, USA
<sup>1</sup>Department of Biomedical Engineering, Johns Hopkins University, Baltimore, MD, USA
<sup>3</sup>Department of Computer Science, Johns Hopkins University, Baltimore, MD, USA

Abstract—Stiffness estimation in ultrasound shear wave elastography critically depends on the quality of shear wave motion fields derived from acoustic radiation force-perturbed ultrasound frames. However, as shear waves propagate through tissue, noise and rigid structures reduce motion amplitudes depending on tissue and acoustic properties. The loss of amplitude degrades shear wave speed estimation and limits the effective field of view. Herein, we introduce ShearMoFit, a dual-plane shear wave motion cleaning technique designed to enhance robustness to noise and amplitude loss. After obtaining motion fields using the Loupas algorithm and applying directional filtering, each time-lateral slice is normalized and summed. A flood-fill algorithm isolates the shear wave trajectory, followed by RANSACbased polynomial fitting across axial-lateral planes. The resulting coordinates define a spatially decaying mask that localizes the shear wavefront while suppressing noise. When applied to a CIRS 059 breast phantom, relative to Loupas-based reconstructions, ShearMoFit improves median signal-to-noise ratios by 13.83 dB in background regions, 22.65 dB in inclusion regions, and improves the median contrast-to-noise ratio by 27.10 dB. These improvements are promising for shear wave motion-tracking driven tissue characterization, enabling more accurate diagnosis, treatment monitoring, and clinical adoption of elastography.

Index Terms—Shear wave elastography, noise robustness, ShearMoFit, shear wave speed, RANSAC, flood-fill

# I. INTRODUCTION

Ultrasound elastography is a non-invasive imaging modality that assesses the mechanical properties of biological tissues by exploiting the differences in elasticity between healthy and pathological regions [1], [2]. Among different ultrasound elastography techniques, shear wave elastography [3], [4] is widely adopted due to its ability to provide quantitative, reproducible, and operator-independent measurements of tissue stiffness. Unlike traditional elastography methods that rely on manual compression and relative deformation [5]-[7], shear wave elastography utilizes an acoustic radiation "push" force to generate shear waves within the tissue. Shear wave elastography has demonstrated promise in a broad range of clinical applications, including liver fibrosis staging, breast tumor characterization, and musculoskeletal evaluations [8]-[10]. One key benefit of shear wave elastography is the ability to provide localized stiffness maps, making this technique a valuable tool for diagnosis, treatment planning, and disease

Initiated with an acoustic radiation push force applied to a tissue medium to induce tissue particle displacement, particle

displacements spread in the form of shear waves at a speed of  $c_s$ . This shear wave speed is related to the tissue medium elasticity through the relation  $E = 3\rho c_s^2$ , where E and  $\rho$ denote medium elasticity modulus and density, respectively [11]. The shear waves are tracked using high-frame-rate (e.g., 3-10 kHz) in-phase/quadrature (IQ) or radio-frequency (RF) ultrasound data. The shear wave motion (i.e., tissue particle displacement or velocity) is then estimated from the IQ or RF data with speckle-tracking algorithms [12]-[19]. Using the tracked particle motion fields, shear wave speed can be estimated through time-of-flight or phase velocity methods [20]–[25]. Due to the sequential steps of tissue particle displacement, followed by shear wave speed estimation, then tissue elasticity estimation, the accuracy of the estimated tissue elasticity heavily depends on the quality of the tracked shear wave motion.

At distant locations from the acoustic push focus (e.g., >2cm, depending on medium properties, acoustic intensity, depth, etc.), shear wave signal attenuation leads to reduced motion amplitudes and a low signal-to-noise ratio (SNR) in speckle-tracked particle displacement estimations. As a result, the accuracy of subsequent shear wave speed estimation is reduced, which, in turn, limits the effective shear wave imaging field. Conventional speckle-tracking methods lack the ability to address low-SNR regions, often resulting in noise-dominated motion estimates and erroneous elasticity maps. To address this, low-SNR regions must be cleaned of noise while preserving the shear wavefront and regenerating low-amplitude shear wave signals.

In this paper, we propose ShearMoFit, a dual-plane shear wave motion cleaning technique designed to improve the accuracy of shear wave speed estimation in noisy and signal attenuated regions. ShearMoFit utilizes spatiotemporal features of the shear wave motion (i.e., tissue particle displacement) by sequentially processing time–lateral and axial–lateral planes. Starting from Loupas-tracked [13] motion. We tested Shear-MoFit using tissue-mimicking phantom data to investigate expected improvements in background and inclusion shear wave speed estimation and benchmark our results against Loupas-tracked motion.

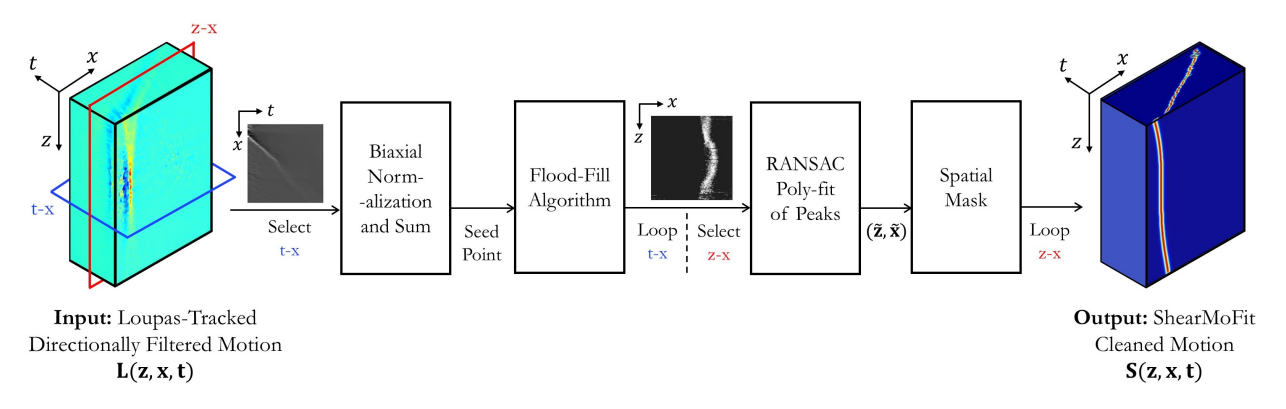


Fig. 1. An illustration of the ShearMoFit strategy.

### II. METHODS

# A. Experimental Phantom Data and Displacement Tracking

A CIRS 059 breast elastography phantom (CIRS Inc., Norfolk, VA, USA) was utilized for data acquisition. This phantom contains multiple inclusions with reported elasticity that is at least twice that of the  $20 \pm 5~\mathrm{kPa}$  background. A Verasonics Vantage 128 (Kirkland, WA) research ultrasound system with an L7-4 linear array transducer (central frequency: 5.2 MHz, sampling frequency: 20.8 MHz, 128 elements, element width: 0.25 mm, pitch: 0.3 mm) was used to acquire data comprising homogeneous tissue and an inclusion surrounded by tissue. The acoustic push force was created with 32 active elements and focused at a depth of 15 mm. IQ data was acquired to track the resulting acoustic response with a frame rate of 10 kHz. Motion tracking was performed with the Loupas algorithm [13], followed by a spatiotemporal median filter with kernel dimensions (z, x, t) = (3, 3, 5) to suppress noise artifacts, where z, x, and t are variables to indicate axial, lateral, and temporal dimensions, respectively. Directional filtering was then applied to remove shear wave components propagating in undesired directions (e.g., reflections between the background and inclusion). The resulting motion volume is denoted as  $\mathbf{L}(z,x,t) \in \mathbb{R}^{Z \times X \times T}$ , where Z, X, and T are the total number of axial pixels, lateral pixels, and temporal samples, respectively.

# B. ShearMoFit

The process of ShearMoFit is depicted in Fig. 1. Each t–x slice of the volume  $\mathbf{L}$  was biaxially normalized by taking each sample located at a particular t value, dividing by the maximum value, then repeating this process for each sample located at a particular x value, resulting in two matrices of normalized t-x values and finally performing summation, as follows

$$P'_{tx}(x,t) = \frac{P_{tx}}{\max_{t}(P_{tx})} + \frac{P_{tx}}{\max_{x}(P_{tx})},\tag{1}$$

where  $P_{tx} \in \mathbb{R}^{T \times X}$  refers to a t-x slice, and the  $\max(\cdot)$  operators normalize  $P_{tx}$  over the time and lateral dimensions. A seed point was determined for each t-x slice by first taking

the maximum value of  $P_{tx}'$  at 2 ms to obtain  $x_s$ , then taking the maximum value of  $P_{tx}'$  at  $x_s$  to obtain  $t_s$ , as follows:

$$x_s = \underset{x}{\operatorname{arg\,max}} P'_{tx}(x, t = 2 \text{ ms}) \tag{2}$$

$$t_s = \underset{t}{\operatorname{arg\,max}} \ P'_{tx}(x = x_s, t) \tag{3}$$

These seed parameters were empirically determined to avoid "blind regions" [26] from the acoustic push. A flood-fill algorithm [27] was then applied to the output of Eq. (1) for each t-x slice, using the identified seed point,  $(x_s,t_s)$ . Each z-x frame was then processed by fitting a 5-th degree polynomial to peak positions using a RANSAC algorithm [28], with axial coordinates as the input. The RANSAC-fitted coordinates ( $\tilde{\mathbf{z}}, \tilde{\mathbf{x}}$ ) define the following 2D mask:

$$W(z,x) = \sum_{i=0}^{Z-1} \exp\left[-\frac{(z-\tilde{\mathbf{z}}_i)^2 + (x-\tilde{\mathbf{x}}_i)^2}{2\varrho^2}\right], \quad (4)$$

where  $\varrho$  is a constant that determines the spatial decay of the mask W(z,x). This RANSAC polynomial fitting was applied to each z-x plane to obtain a volume representation  $\mathbf{S}(z,x,t) \in \mathbb{R}^{Z \times X \times T}$ . The entire process of taking  $\mathbf{L}(z,x,t)$  as input to generate  $\mathbf{S}(z,x,t)$  is referred to as ShearMoFit.

# C. Shear Wave Speed Estimation and Metrics

A cross-correlation-based [21] time-of-flight method was employed to estimate the shear wave speed from Loupas tracked motion, L, and ShearMoFit processed motion, S. Signal-to-noise ratio (SNR) and contrast-to-noise ratio (CNR) were calculated as defined below:

$$SNR = 20 \log_{10} \left(\frac{\mu}{\sigma}\right) [dB] \tag{5}$$

CNR = 
$$20 \log_{10} \left( \frac{|\mu_{t} - \mu_{b}|}{\frac{1}{2} \sqrt{\sigma_{t}^{2} + \sigma_{b}^{2}}} \right) [dB]$$
 (6)

where  $\mu$  and  $\sigma$  denote the mean and standard deviation of a shear wave speed estimated region and the subscripts t and b represent the target and background, respectively. A total of 24 2 mm  $\times$  2 mm background regions of interest (ROIs) and five 2 mm  $\times$  2 mm target ROIs (located within an imaged inclusion) were selected. All data processing and analyses were performed with Python v3.12.

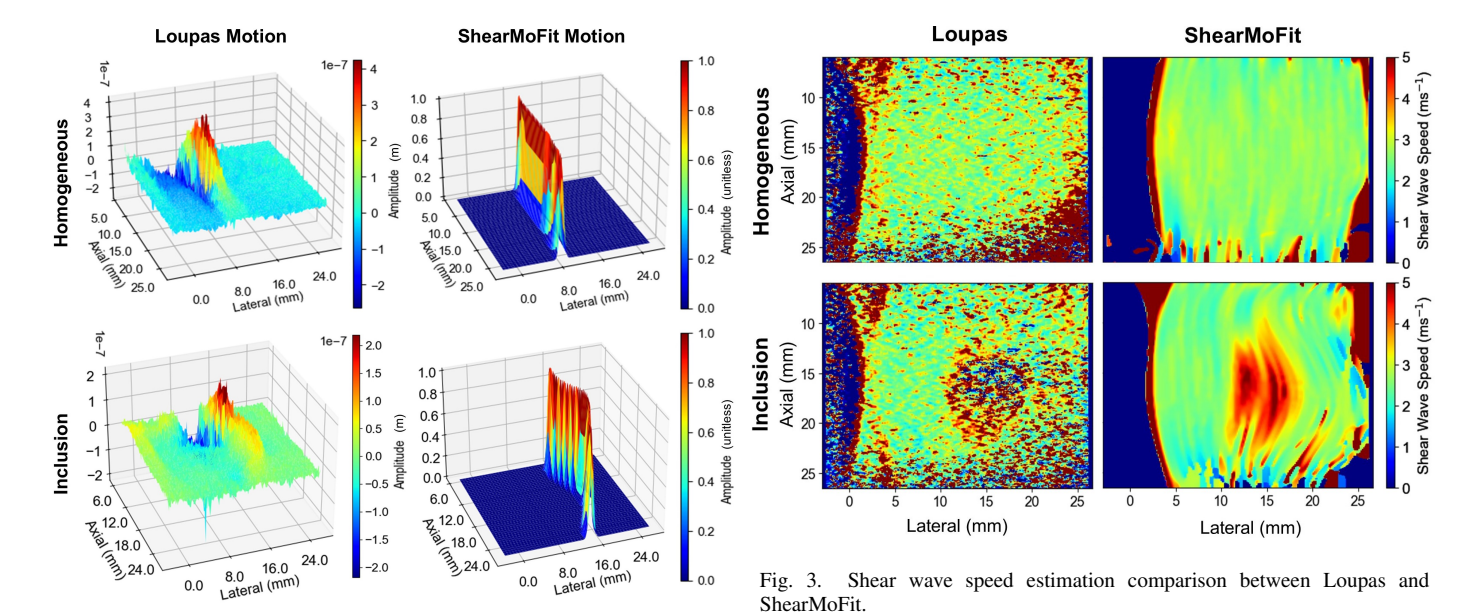


Fig. 2. Shear wave motion comparison between Loupas and ShearMoFit.

# III. RESULTS

Fig. 2 shows the shear wave motions obtained with the Loupas (left) and ShearMoFit (right) methods algorithms applied to a homogeneous (top) elasticity region and a region containing an inclusion (bottom). In the homogeneous case, the Loupas algorithm produced amplitude variations and background noise, whereas ShearMoFit presents a cleaner and more sharply defined wavefront with consistent amplitude. In the inclusion case, the Loupas algorithm outputs a decayed shear wave front surrounded by noise, whereas ShearMoFit displays a cleaner signal.

Fig. 3 shows images of shear wave speeds estimated using the Loupas and ShearMoFit algorithms. The Loupas-based shear wave speed maps are noisy and contain higher than expected estimation in the background regions and lower than expected background estimations within the inclusion. In comparison, the ShearMoFit shear wave speed maps are smoother and contain less variations throughout the field-of-view.

Fig. 4 shows SNR and CNR measurements. Relative to the Loupas algorithm, ShearMoFit improves the median SNR by 13.83 dB and 22.65 dB in the background and target, respectively. The corresponding median CNR improvement is 27.10 dB.

## IV. DISCUSSION

This work is the first to propose a dual-plane ultrasound shear wave motion cleaning technique that enhances motion quality and subsequent shear wave speed estimation. By combining time-lateral flood-fill and axial-lateral RANSAC-based polynomial fitting, our method suppresses noise and localizes the shear wavefronts. Compared to the conventional Loupas tracking algorithm, the improved signal quality and shear wave speed estimation with ShearMoFit (Figs. 2-4) highlights its

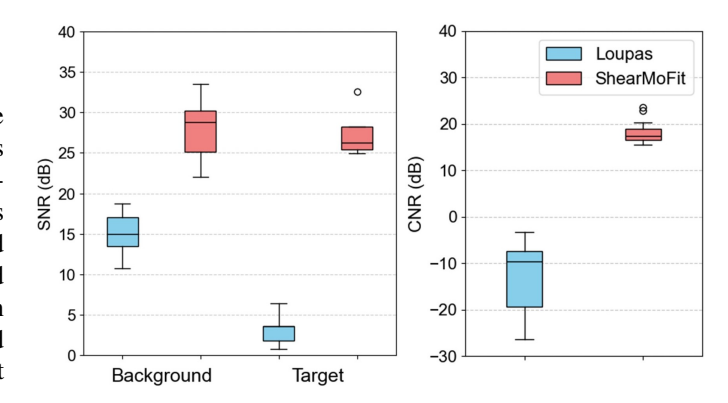


Fig. 4. SNR and CNR comparison between Loupas and ShearMoFit.

potential to improve stiffness imaging accuracy and support broader clinical adoption of shear wave elastography.

The field-of-view improvement (e.g., bottom right regions of estimated shear wave speed in Fig. 3) indicates that the Loupas algorithm overestimates the expected shear wave speed, due to low-amplitude signals being dominated by noise. ShearMoFit partially recovers the corrupted information in this bottom-right region, producing usable shear wave speed quantities by cleaning the shear wave signals with masks (Fig. 3).

One limitation of ShearMoFit is the artifacts observed near the proximal and distal regions of the inclusion in Fig. 3. These artifacts occur because of Runge's phenomenon [29], which is a common issue when using high-degree polynomial fitting. As ShearMoFit relies on RANSAC-based polynomial modeling to trace the wavefront trajectory, the choice of polynomial degree plays a critical role in controlling such artifacts, resulting in streak-like distortions near the proximal and distal inclusion boundaries. These artifacts can potentially be improved with adaptive or regularization strategies in future work.

# V. CONCLUSION

This work presents ShearMoFit, a novel dual-plane ultrasound shear wave motion cleaning technique to improve motion field fidelity and shear wave speed estimation in elastography. By combining time-lateral flood-fill segmentation with axial-lateral RANSAC-based polynomial fitting, ShearMoFit effectively localizes shear wave propagation and suppresses noise. Experimental results demonstrate median improvements of 13.83 dB, 22.65 dB, and 27.10 dB in background SNR, target SNR, and CNR, respectively, compared to conventional Loupas-based tracking. In addition, ShearMoFit improves the spatial field-of-view of the estimated shear wave speed map, relative to the correponding map produced by the Loupas algorithm. These improvements are promising for more reliable elasticity measurements, supporting enhanced detection and characterization of pathological tissue stiffness, which has the potential to facilitate more robust clinical decision-making in ultrasound-based disease assessment.

### ACKNOWLEDGMENTS

This work is supported by the National Institute of Biomedical Imaging and Bioengineering of the National Institutes of Health under Award Number R01EB032960.

### REFERENCES

- [1] T. Shiina, K. R. Nightingale, M. L. Palmeri, T. J. Hall, J. C. Bamber, R. G. Barr, L. Castera, B. I. Choi, Y.-H. Chou, D. Cosgrove et al., "Wfumb guidelines and recommendations for clinical use of ultrasound elastography: Part 1: basic principles and terminology," Ultrasound in Medicine & Biology, vol. 41, no. 5, pp. 1126–1147, 2015.
- [2] R. G. Barr, K. Nakashima, D. Amy, D. Cosgrove, A. Farrokh, F. Schafer, J. C. Bamber, L. Castera, B. I. Choi, Y.-H. Chou et al., "Wfumb guidelines and recommendations for clinical use of ultrasound elastography: Part 2: breast," *Ultrasound in Medicine & Biology*, vol. 41, no. 5, pp. 1148–1160, 2015.
- [3] A. P. Sarvazyan, O. V. Rudenko, S. D. Swanson, J. B. Fowlkes, and S. Y. Emelianov, "Shear wave elasticity imaging: a new ultrasonic technology of medical diagnostics," *Ultrasound in Medicine & Biology*, vol. 24, no. 9, pp. 1419–1435, 1998.
- [4] M. Ashikuzzaman and M. A. Lediju Bell, "L1-norm-regularized particle motion estimation in ultrasound shear wave elastography," in 2024 IEEE Ultrasonics, Ferroelectrics, and Frequency Control Joint Symposium (UFFC-JS), 2024, pp. 1–4.
- [5] M. Ashikuzzaman, A. Sharma, N. Venkatayogi, E. Oluyemi, K. Myers, E. Ambinder, H. Rivaz, and M. A. L. Bell, "Mixture: L1-norm-based mixed second-order continuity in strain tensor ultrasound elastography," *IEEE Transactions on Ultrasonics, Ferroelectrics, and Frequency Con*trol, 2024.
- [6] M. Ashikuzzaman, A. K. Tehrani, and H. Rivaz, "Exploiting mechanics-based priors for lateral displacement estimation in ultrasound elastography," *IEEE Transactions on Medical Imaging*, vol. 42, no. 11, pp. 3307–3322, 2023
- [7] M. Ashikuzzaman, B. Peng, J. Jiang, and H. Rivaz, "Alternating direction method of multipliers for displacement estimation in ultrasound strain elastography," *Medical Physics*, vol. 51, no. 5, pp. 3521–3540, 2024.
- [8] A. Kovatsch, H. Honcharova-Biletska, D. Segna, K. Steigmiller, S. Blümel, R. A. Deibel, T. Kühlewindt, G. Leinenkugel, S. Müller, E. Furrer et al., "Performance of two-dimensional shear wave elastography and transient elastography compared to liver biopsy for staging of liver fibrosis," European Journal of Clinical Investigation, vol. 53, no. 7, p. e13980, 2023.
- [9] J. Gu, R. Ternifi, N. B. Larson, J. M. Carter, J. C. Boughey, D. L. Stan, R. T. Fazzio, M. Fatemi, and A. Alizad, "Hybrid high-definition microvessel imaging/shear wave elastography improves breast lesion characterization," *Breast Cancer Research*, vol. 24, no. 1, p. 16, 2022.

- [10] A. N. Koruyucu and F. Aşantoğrol, "Determination of masseter and temporal muscle thickness by ultrasound and muscle hardness by shear wave elastography in healthy adults as reference values," *Dentomaxillofacial Radiology*, vol. 53, no. 2, pp. 137–152, 2024.
- [11] J. Bercoff, M. Tanter, and M. Fink, "Supersonic shear imaging: a new technique for soft tissue elasticity mapping," *IEEE Transactions on Ultrasonics, Ferroelectrics, and Frequency Control*, vol. 51, no. 4, pp. 396–409, 2004.
- [12] M. Ashikuzzaman, A. Héroux, A. Tang, G. Cloutier, and H. Rivaz, "Displacement tracking techniques in ultrasound elastography: From cross correlation to deep learning," *IEEE Transactions on Ultrasonics*, Ferroelectrics, and Frequency Control, vol. 71, no. 7, pp. 842–871, 2024.
- [13] T. Loupas, J. Powers, and R. W. Gill, "An axial velocity estimator for ultrasound blood flow imaging, based on a full evaluation of the doppler equation by means of a two-dimensional autocorrelation approach," *IEEE Transactions on Ultrasonics, Ferroelectrics, and Frequency Con*trol, vol. 42, no. 4, pp. 672–688, 1995.
- [14] M. Ashikuzzaman, J. Huang, S. Bonwit, A. Etemadimanesh, P. Raghavan, and M. A. L. Bell, "Deep learning-based displacement tracking for post-stroke myofascial shear strain quantification," in 2024 IEEE International Symposium on Biomedical Imaging. IEEE, 2024, pp. 1–4.
- [15] M. Ashikuzzaman, H. Rivaz, and M. A. L. Bell, "Two-dimensional displacement estimation using mixed second-order regularization in total variation-based ultrasound elastography," in *Medical Imaging 2024: Ultrasonic Imaging and Tomography*, vol. 12932. SPIE, 2024, pp. 45–50.
- [16] M. G. Kibria and M. K. Hasan, "A class of kernel based real-time elastography algorithms," *Ultrasonics*, vol. 61, pp. 88–102, 2015.
- [17] M. Ashikuzzaman, J. Huang, S. Bonwit, A. Etemadimanesh, P. Raghavan, and M. A. L. Bell, "Displacement tracking reliability in muscle shear strain quantification," in *Medical Imaging 2024: Ultrasonic Imaging and Tomography*, vol. 12932. SPIE, 2024, pp. 66–71.
- [18] B. Peng, Y. Xian, Q. Zhang, and J. Jiang, "Neural-network-based motion tracking for breast ultrasound strain elastography: An initial assessment of performance and feasibility," *Ultrasonic Imaging*, vol. 42, no. 2, pp. 74–91, 2020.
- [19] M. Ashikuzzaman and H. Rivaz, "Second-order ultrasound elastography with 11-norm spatial regularization," *IEEE Transactions on Ultrasonics*, Ferroelectrics, and Frequency Control, vol. 69, no. 3, pp. 1008–1019, 2022.
- [20] M. L. Palmeri, M. H. Wang, J. J. Dahl, K. D. Frinkley, and K. R. Nightingale, "Quantifying hepatic shear modulus in vivo using acoustic radiation force," *Ultrasound in Medicine & Biology*, vol. 34, no. 4, pp. 546–558, 2008.
- [21] M. Tanter, J. Bercoff, A. Athanasiou, T. Deffieux, J.-L. Gennisson, G. Montaldo, M. Muller, A. Tardivon, and M. Fink, "Quantitative assessment of breast lesion viscoelasticity: initial clinical results using supersonic shear imaging," *Ultrasound in Medicine & Biology*, vol. 34, no. 9, pp. 1373–1386, 2008.
- [22] M. H. Wang, M. L. Palmeri, V. M. Rotemberg, N. C. Rouze, and K. R. Nightingale, "Improving the robustness of time-of-flight based shear wave speed reconstruction methods using ransac in human liver in vivo," *Ultrasound in Medicine & Biology*, vol. 36, no. 5, pp. 802–813, 2010.
- [23] J. Brum, M. Bernal, J.-L. Gennisson, and M. Tanter, "In vivo evaluation of the elastic anisotropy of the human achilles tendon using shear wave dispersion analysis," *Phys Med Biol*, vol. 59, no. 3, p. 505, 2014.
- [24] P. Kijanka, B. Qiang, P. Song, C. A. Carrascal, S. Chen, and M. W. Urban, "Robust phase velocity dispersion estimation of viscoelastic materials used for medical applications based on the multiple signal classification method," *IEEE Transactions on Ultrasonics, Ferroelectrics, and Frequency Control*, vol. 65, no. 3, pp. 423–439, 2018.
- [25] M. J. Alam and M. K. Hasan, "A constrained optimization approach for ultrasound shear wave speed estimation with time-lateral plane cleaning," arXiv preprint arXiv:2407.20561, 2024.
- [26] T. Nordenfur, "Comparison of pushing sequences for shear wave elastography," 2013.
- [27] M. C. Codrea and O. S. Nevalainen, "Note: An algorithm for contour-based region filling," *Computers & Graphics*, vol. 29, no. 3, pp. 441–450, 2005.
- [28] K. G. Derpanis, "Overview of the ransac algorithm," *Image Rochester NY*, vol. 4, no. 1, pp. 2–3, 2010.
- [29] B. Fornberg and J. Zuev, "The runge phenomenon and spatially variable shape parameters in rbf interpolation," *Computers & Mathematics with Applications*, vol. 54, no. 3, pp. 379–398, 2007.